Is FIRST J102347.6+003841 Really a Cataclysmic Binary?

John R. Thorstensen
Dartmouth College

Eve Armstrong
Columbia University

IS FIRST J102347.6+003841 REALLY A CATACLYSMIC BINARY?[1]

John R. Thorstensen

Department of Physics and Astronomy, 6127 Wilder Laboratory, Dartmouth College, Hanover, NH 03755-3528;
john.thorstensen@dartmouth.edu

and

Eve Armstrong

Department of Astronomy, Columbia University, 550 West 120th Street, New York, NY 10027

ABSTRACT

The radio source FIRST J102347.6+003841 was presented as the first radio-selected cataclysmic variable star. In the discovery paper, Bond et al. (2002) show a spectrum consistent with a magnetic AM Her–type system, or polar, featuring strong Balmer lines, He I and He II emission lines, and a light curve with rapid, irregular flickering. In contrast, Woudt, Warner, and Pretorius found a smoothly varying light curve with a period near 4.75 hr and one minimum per orbit, indicating that the state of the system had changed dramatically. We present time-resolved spectra showing a superficially normal, mid-G type photosphere, with no detectable emission lines. The absorption-line radial velocity varies sinusoidally, with semiamplitude 268 ± 4 km s^{-1}, on the orbital period, which is refined to 0.198094(2) days. At this orbital period, the secondary's spectral type is atypically early, suggesting an unusual evolutionary history. We also obtained photometry around the orbit in B, V, and I. The light curve resembles that observed by Woudt, Warner, and Pretorius, and the colors are modulated in a manner consistent with a heating effect. A simple illumination model matches the observations strikingly well, with a Roche lobe–filling secondary near $T_{\mathrm{eff}} = 5650$ K being illuminated by a primary with an isotropic luminosity of $\sim 2\,L_{\odot}$. The modest amplitude of the observed modulation constrains the orbital inclination $i \sim 55°$ or less, unless the gravity darkening is artificially reduced. Combining the low i with the secondary's velocity amplitude gives a primary star mass above the Chandrasekhar limit when conventional gravity darkening is assumed. We consider the robustness of this conclusion and examine the possibility that the compact object in this system is not a white dwarf, in which case this is not actually a cataclysmic variable. On close examination, FIRST J102347.6+003841 defies easy classification.

Key words: binaries: close — novae, cataclysmic variables — stars: individual (FIRST J102347.6+003841) — stars: neutron

1. INTRODUCTION

Cataclysmic variable stars (CVs) are close binaries in which a white dwarf accretes matter from a less-evolved companion (the secondary), which usually resembles a lower main-sequence star. CVs have a rich phenomenology, and the theory of CVs ranges across wide areas of astrophysics; Warner (1995) presents a comprehensive review.

CVs draw attention to themselves through a variety of channels, most importantly through variability (especially for novae and dwarf novae), X-ray flux, unusual optical colors, or emission-line spectra. Magnetic CVs are sometimes weak radio sources, and the subject of this paper, FIRST J102347.6+003841 (hereafter FIRST 1023+00), is thought to be the only CV that was initially found from its radio flux. Bond et al. (2002) identified the radio source with a 17th magnitude, flickering star, the spectrum of which showed emission lines typical of an AM Her class CV, or "polar." The object was independently discovered in the Sloan Digital Sky Survey (SDSS); Szkody et al. (2003) show a spectrum with a strong blue continuum and high-excitation emission lines. They remark that the lines are not as strong as in typical AM Her stars (polars), but suggest that the system might be a DQ Her star (or "intermediate polar"). Woudt et al. (2004) obtained photometry showing a smooth light curve with a period

of 4.75 hr, in sharp contrast to the flickering seen by Bond et al. (2002). They attribute the modulation to a heating (sometimes called reflection) effect. The very different photometric behavior seen by Woudt et al. (2004) suggests that FIRST 1023+00 undergoes dramatic changes in state. The SDSS data already suggest such a conclusion, as the broadband colors are rather red (Table 1 of Szkody et al. 2003) but the spectrum (which was not simultaneous with the photometry) appears quite blue (Fig. 2 of their paper).

Here we present spectra that show only late-type absorption features, dramatically different from the spectra published by Bond et al. (2002) and Szkody et al. (2003). The radial velocity of the late-type spectrum is modulated on the 4.75 hr photometric period, which allows us to refine the ephemeris and constrain the dynamics. The spectral type and color of the late-type star are atypically early for the orbital period, suggesting that it began mass transfer after significant nuclear evolution had taken place. We also present time-resolved BVI photometry, which shows an orbital color modulation consistent with a heating effect. We model this effect quantitatively in the Roche geometry. These models, together with the completely atypical quiescent behavior of this system, suggest a radically different interpretation of the object, in which the compact object is a neutron star or a black hole.

2. OBSERVATIONS

Table 1 contains a journal of the observations. A single survey spectrum was taken in 2003 January, which showed only

---

TABLE 1
JOURNAL OF OBSERVATIONS

Date (UT)	N	HA (start) (hh:mm)	HA (end) (hh:mm)
Spectroscopy (2.4 m)			
2003 Jan 31...............	1	−0:13	−0:13
2004 Jan 18...............	4	+0:17	+1:30
2004 Jan 19...............	11	−3:52	+3:06
2004 Jan 20...............	1	+2:38	+2:38
2004 Mar 8	1	−4:07	−4:07
2004 Mar 9	12	−3:59	+1:32
2004 Nov 18.............	3	−1:22	−0:58
Filter Photometry (2.4 m)			
2004 Feb 29...............	12	−1:07	−0:41
I Time-series Photometry (2.4 m)			
2004 Feb 29...............	5	−0:37	+4:00
2004 Mar 1	23	−3:15	+4:15
BVI Time-series Photometry (1.3 m)			
2004 May 12..............	42	+0:50	+4:10
2004 May 16..............	38	+1:16	+4:13
2004 May 20..............	39	+1:15	+4:17

TABLE 2
FILTER PHOTOMETRY

α[a]	δ[a]	$U - B$	$B - V$	V	$V - I$
Field Stars					
10 23 39.24........	+00 40 49.4	−0.32	0.46	19.20	0.63
10 23 40.40........	+00 39 29.2	. . .	0.98	18.59	1.14
10 23 43.31........	+00 38 19.5	0.12	0.69	14.86	0.80
10 23 47.03........	+00 39 08.7	. . .	1.20	17.69	1.39
10 23 50.53........	+00 38 16.6	. . .	1.54	19.20	2.43
10 23 50.69........	+00 37 38.7	−0.03	0.58	17.40	0.68
10 23 50.90........	+00 37 16.7	. . .	1.17	19.06	1.41
10 23 55.67........	+00 39 27.3	. . .	1.27	18.76	1.46
10 23 56.13........	+00 36 52.3	0.37	0.86	16.56	1.02
Variable Star					
10 23 47.70........	+00 38 41.2	0.31	0.69	17.46:[b]	0.78

[a] Coordinates refer to the ICRS, and are from a fit to 11 USNO A2.0 stars, with a scatter of 0″.4. Units of right ascension are hours, minutes, and seconds, and units of declination are degrees, arcminutes, and arcseconds.

[b] The colon indicates that the star is variable.

absorption lines. We initially thought we had observed the wrong star. Further observations in 2004 January showed that there was no error in the identification and revealed the periodicity in the absorption velocity. We obtained more spectroscopy in 2004 March, but poor weather limited the coverage. Also in 2004 March, we obtained photometry and some differential time-series photometry. In 2004 May, near the end of the observing season, we obtained differential time-series *BVI* filter photometry covering the entire orbit.

2.1. Spectroscopy

The spectroscopic protocols were for the most part identical to those described in Thorstensen et al. (2004). Briefly, we used the "modular" spectrograph, a 600 line mm^{-1} grating, and a SITe 2048^2 CCD. This yielded 2 Å pixel^{-1} from 4210 to 7560 Å (vignetting severely toward the ends) and a typical resolution of 3.5 Å FWHM. The spectra were flux-calibrated using observations of standard stars, but spectrophotometry was approximate because of uncalibratable losses at the 1″ slit, occasional cloud, and an instrumental effect of uncertain origin that sometimes introduces wavelike distortions in stellar continua.

For absorption-line radial velocity measurements we used the cross-correlation method of Tonry & Davis (1979), as implemented by Kurtz & Mink (1998) in the RVSAO package. The cross-correlation template was a composite of many IAU velocity standard spectra, as described in Thorstensen et al. (2004).

2.2. Photometry

In 2004 March we obtained direct images, including three contiguous sets of *UBVI* images, with the Hiltner 2.4 m telescope and a SITe 2048^2 CCD detector that gave 0″.275 pixel^{-1}. We derived standard magnitudes from observations of Landolt (1992) standard-star fields; Table 2 gives the results. The magnitude transformations had standard deviations <0.02 mag for V, $B - V$, and $V - I$, but 0.08 mag for $U - B$ (which often gives

large scatter). For the brightest stars, the magnitudes and colors from the three image sets agreed to ∼0.01 mag, indicating that conditions were clear. Figure 1 shows the stars measured and their magnitudes. In addition to the standardized photometry, we took 28 *I*-band "snapshots" over two nights in order to sample the light curve and establish the relationship between photometric and spectroscopic phase. These were reduced using the IRAF implementation of DAOPHOT in a semiautomated mode. The differential magnitudes were converted to approximate standard *I* magnitudes using the photometric sequence.

We obtained more extensive time-series photometry of the object on three nights in 2004 May using the 1.3 m McGraw-Hill Telescope and a thinned SITe 1024^2 CCD. To minimize dead time, we binned the readout 2 × 2 and cropped the area to
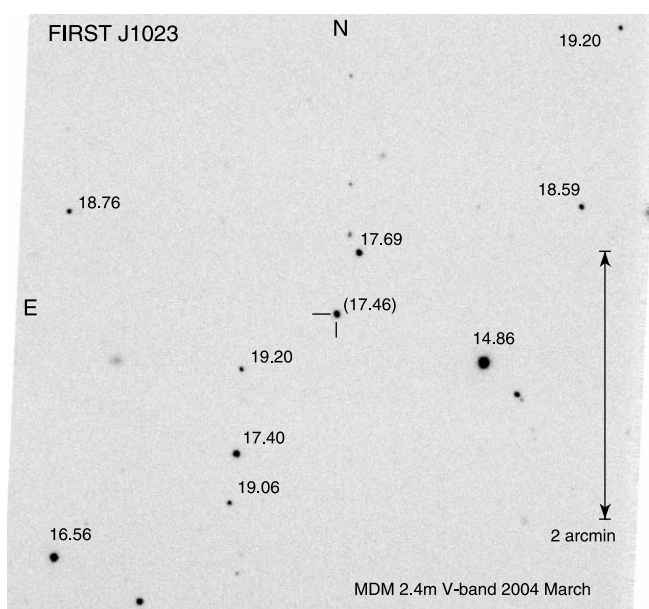

FIG. 1.—Finding chart for FIRST 1023+00 from the median of three *V*-band images taken in 2004 March. Stars are labeled with their *V* magnitudes, and FIRST 1023+00 is indicated by the two short lines. Scale and orientation are as indicated.
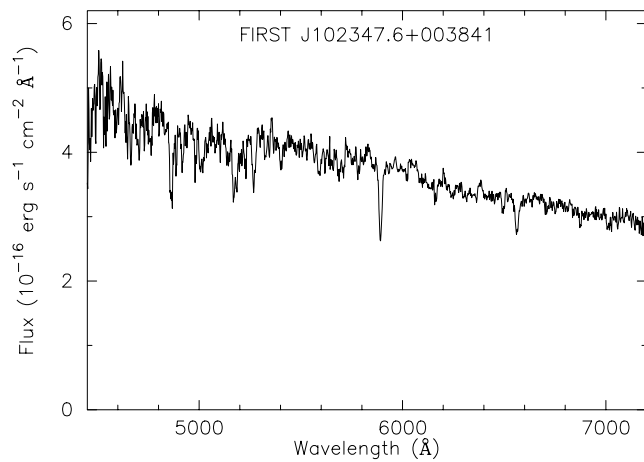
Fig. 2.—Mean spectrum of FIRST 1023+00.

yield a 256^2 image with a scale of $1''.018$ per (binned) pixel. We cycled through 120 s exposures in the B filter and 60 s exposures in V and I filters. After bias subtraction and flat fielding using twilight sky exposures, we measured magnitudes in $4''$ diameter apertures using IRAF. Differential magnitudes were computed relative to the $V = 14.86$ comparison star west of the variable (see Fig. 1). The $V = 17.40$ mag star to the southeast served as a check; typical precisions were <0.02 mag (after we discarded a few images taken through intermittent heavy cloud). Hour angle constraints prevented us from covering the entire orbit in one night, but we were able to piece together coverage of the whole orbit from the three nights' data. When phase redundancy was obtained, the different nights agreed closely—there was no trace of secular variability. The differential magnitudes and colors were standardized using the sequence in Table 2.

3. RESULTS AND ANALYSIS

Figure 2 shows the mean spectrum, shifted to the rest frame of the secondary using the ephemeris described later. It is essentially that of a late-type star, with no emission lines. The flux level implies $V = 17.5$, in good agreement with the filter photometry.

TABLE 3
RADIAL VELOCITIES

Time[a]	v_{abs} (km s^{-1})	σ (km s^{-1})	Time[a]	v_{abs} (km s^{-1})	σ (km s^{-1})
52670.8778.....	211	16	53024.0480.....	245	10
53022.9338.....	−111	12	53025.0261.....	173	14
53022.9722.....	−274	12	53072.6158.....	173	29
53022.9784.....	−275	13	53073.6184.....	127	12
53022.9845.....	−234	10	53073.6294.....	18	12
53023.7589.....	−266	12	53073.6404.....	−77	12
53023.7678.....	−284	10	53073.6514.....	−165	11
53023.8092.....	−5	10	53073.6644.....	−230	12
53023.8522.....	252	9	53073.6754.....	−265	10
53023.8944.....	144	10	53073.7901.....	282	13
53023.9037.....	71	11	53073.8012.....	232	17
53023.9351.....	−160	9	53073.8122.....	131	16
53023.9648.....	−257	10	53073.8232.....	63	18
53023.9769.....	−230	9	53073.8370.....	−43	15
53024.0391.....	209	9	53073.8478.....	−115	15

NOTES.—Absorption radial velocities. The uncertainties are from the cross-correlation routine.
[a] Heliocentric Julian Date of midexposure minus 2,400,000.

TABLE 4
FIT TO THE RADIAL VELOCITIES

T_0[a]	P (days)	K (km s^{-1})	γ (km s^{-1})	N	σ[b] (km s^{-1})
53025.0008(5).......	0.198094(2)	268(4)	1(3)	30	14

NOTE.—Parameters of least-squares sinusoid fits to the radial velocities, of the form $v(t) = \gamma + K \sin [2\pi(t - T_0)]/P$.
[a] Heliocentric Julian Date minus 2,452,000.
[b] The rms residual of the fit.

Table 3 lists the cross-correlation radial velocities. A search of these yields a strong periodicity near 4.75 hr, but with several possible precise periods corresponding to different choices of cycle count over the 50 day interval between 2004 January and March. Fortunately, the photometric period published by Woudt et al. (2004) is consistent with only one of the precise periods. Once the 50 day cycle count is decided, the ephemeris extends unambiguously back to the single 2003 January point, further tightening the period. To help us verify the ephemeris, P. Woudt kindly sent the time-series photometry data used by Woudt et al. (2004); combining this with our own time-series photometry again yielded the same period, confirming the ephemeris. The period found here differs slightly from that found by Woudt et al. (2004) from their photometric data alone; our period supersedes theirs, since it is based on a longer time span and has greater redundancy. Table 4 gives the parameters of the best-fitting sinusoid, and Figure 3 shows the folded velocities with the sinusoid superposed.

Figure 4 shows the 1.3 m time-series photometry folded on the spectroscopic ephemeris, in which phase zero corresponds to the inferior conjunction of the secondary star. The light curve is similar to that found by Woudt et al. (2004). Minimum light corresponds closely with inferior conjunction, as expected for a heating effect. The $B - V$ and $V - I$ colors are also modulated, with the star bluest at maximum light. The curves in Figure 4 are from a model described later.

We rectified all the spectra and created the phase-averaged gray-scale representation shown in Figure 5. The most remarkable feature is the complete absence of *any* emission lines. Gray-scale representations of this kind can sometimes bring out subtle spectral features, but this looks remarkably ordinary. There is also no strong modulation of the spectrum around the orbit. The coverage is unfortunately nonuniform (refer to Fig. 3); for a
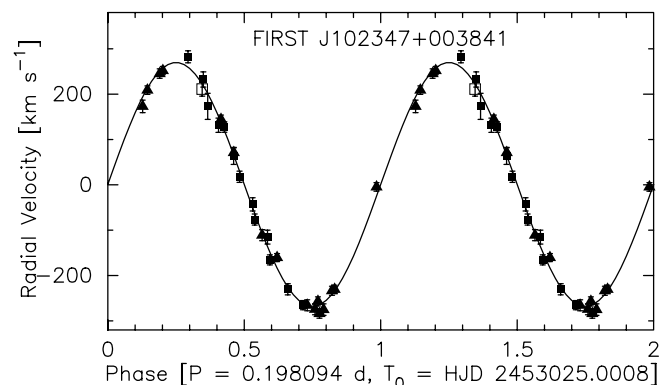

Fig. 3.—Absorption radial velocities folded on the best-fit period, with the best-fit sinusoid superposed. All data are plotted twice for continuity. Filled triangles are from 2004 January, filled squares are from 2004 March, and the open square is the single point from 2003 January.
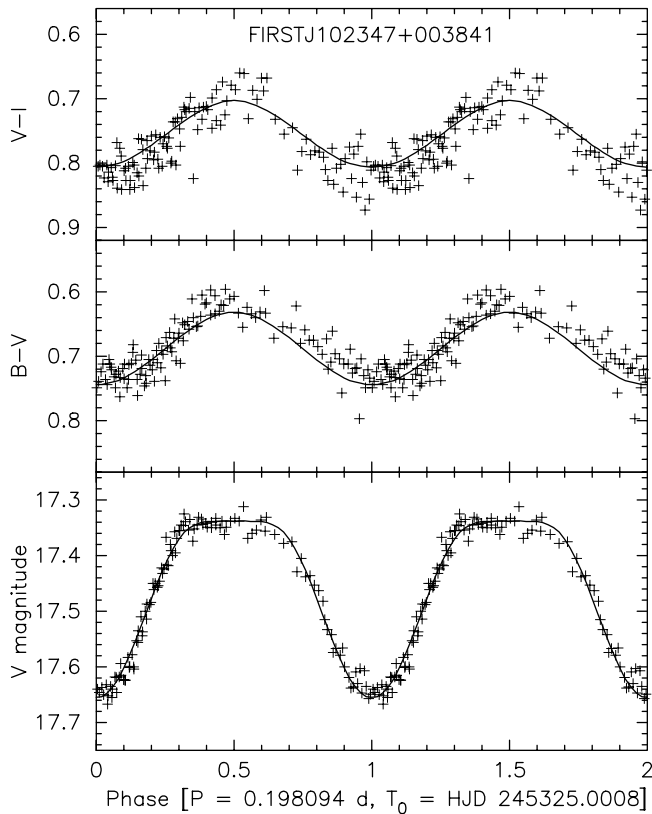
Fig. 4.—Time-series photometry from 2004 May. The vertical scales are adjusted to match the filter photometry of the field. The horizontal axis gives phase in the *spectroscopic* ephemeris, so zero phase corresponds to the inferior conjunction of the absorption-line source. All points are shown twice for continuity. The solid curve is calculated from the heating effect model discussed in the text; this fit is for $M_1 = 2 \, M_\odot$, $M_2 = 0.7 \, M_\odot$, $i = 39°$, $T_{\mathrm{eff},0} = 5691$ K, and $L_1 = 2.45 \, L_\odot$.

Jacoby et al. (1984). These matched reasonably well around mid-G, but with a significant mismatch at the sodium D lines, which are stronger than they should be for the spectral type. The decomposition was consistent with *all* the light coming from the secondary star—there was no need to include any contribution from a hot component. This conclusion is corroborated by the colors in Table 2 and the $V - H$ and $V - J$ colors found by combining the present data with the J and H magnitudes from the 2MASS All Sky Data Release. Pickles (1998) tabulates normal G-dwarf colors in many passbands, and the observed colors are all consistent with a type between G5 and G7. Remarkably, this is even true for the U band, in which one might expect to start seeing a hot component if one were present. Although the phase-averaged spectrum is not sensitive enough to show spectral type variation, the color modulation corresponds to a half-amplitude of around three subtypes, corresponding to ~180 K around mid-G.

4. A LIGHT-CURVE MODELING PROGRAM

The remarkable light and color curve of this system motivated us to construct a light-curve modeling program. In our model, the secondary fills its Roche critical lobe, as CV secondaries generally do; although mass transfer was not evident during our observations, the secondary should still nearly fill its Roche lobe, since the system was actively transferring mass within the last few years and the Kelvin-Helmholtz relaxation time of the secondary's envelope should be much longer than that.

To tessellate the model secondary, we used an icosahedron-based geodesic dome construction similar to (but less elaborate than) that advocated by Hendry & Mochnacki (1992). Each face of the icosahedron was divided into 25 subtriangles, and the vertices were then "pushed out" to the Roche surface to form a 500 sided polyhedron. A vertex of the icosahedron was oriented toward the primary, so that the "pointy" part of the Roche lobe near the inner Lagrangian point was modeled adequately. Figure 6 shows the geometry used for the model secondary.

We define the "base" effective temperature of the secondary, $T_{\mathrm{eff},0}$, as the effective temperature in the absence of gravity darkening or heating effects. The local gravity g at each segment was computed (at the segment's center) and used to determine the gravity darkening through $(T/T_{\mathrm{eff},0}) = (g/\bar{g})^\alpha$. For our standard models we used $\alpha = 0.08$, as recommended by Lucy (1967) for stars with convective envelopes. For limb darkening we used a simple linear law, $I(\mu)/I_0 = 1 - x(1 - \mu)$, where μ is the cosine of the angle away from the local vertical (as is standard) and x is the linear limb-darkening coefficient, which we took to be 0.5 for our standard models. More elaborate limb-darkening laws can

portion of the figure around phase 1, only one observation contributes, so the data remain unchanged with phase. However, coverage is densest on the descending side of the velocity curve, which corresponds to superior conjunction of the secondary. This is the portion of the orbit where the heated face of the secondary is turned toward us, and we still do not see any emission lines.

To estimate the mean spectral type of the secondary, we used the spectral decomposition procedure outlined in Thorstensen et al. (2004), basically subtracting scaled versions of spectral type standard stars away from the mean spectrum and looking for good cancellation of the late-type features. The K- and M-dwarf library spectra taken with the same instrument proved to be too cool to match, so we used G-type library spectra from
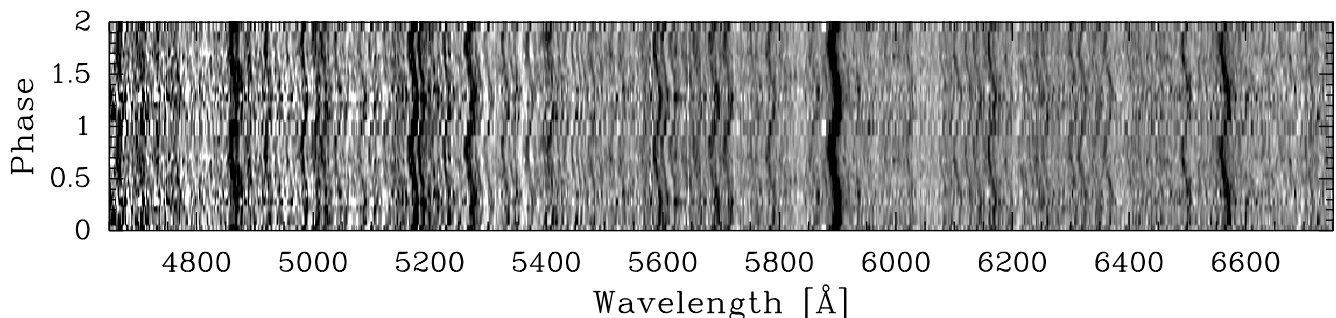

Fig. 5.—Gray-scale representation of the spectra from 2004 March, arranged according to orbital phase. The data are repeated to maintain phase continuity. The gray scale is positive (dark = absorption), and no emission lines are visible. The phase coverage is nonuniform because of weather.
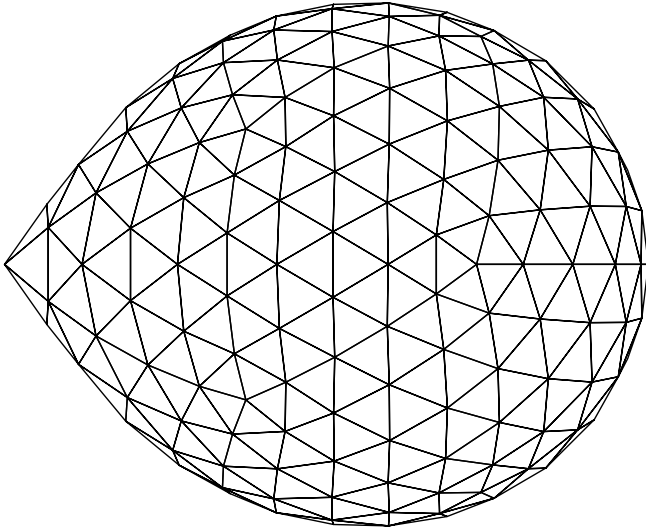
Fig. 6.—Icosahedral tessellation of the secondary used in the light-curve modeling. This view is perpendicular to the orbit plane and corresponds to a mass ratio $q = M_2/M_{wd} = 2/3$.

be justified (Van Hamme 1993), but we chose this for simplicity. To explore the effects of limb- and gravity-darkening, we also computed models with $\alpha = 0$ and 0.16 and models with $x = 0$ and 0.75.

The radiation illuminating the model secondary is assumed to come from the primary star's location, and the primary is assumed to act as a point source. The incident radiation was assumed to thermalize completely and be reradiated in a manner similar to a normal stellar atmosphere, so that the effect of the irradiation could be adequately treated as an increase in the local effective temperature sufficient to carry the added luminosity. This assumption may be questionable, but in the absence of any information about the spectrum of the incident radiation it seemed to be a good starting point.

Once the effective temperature of each segment was determined, the surface brightness in V radiated perpendicular to each segment was estimated based on stellar atmosphere models. More specifically, we computed the quantity S_V, which we define as the absolute V magnitude of a 1 $R_\odot$ star of the same surface brightness; this is

$$S_V = 42.367 - BC(V) - 10 \log T_{eff},$$

where $BC(V)$ is the bolometric correction in the V band. Bessell et al. (1998) give a convenient tabulation of $BC(V)$ versus T_{eff} for ATLAS9 models computed using Kurucz's codes; we created polynomial approximations to the S_V–log T_{eff} relation, and similarly for $B - V$ and $V - I$ (which are also tabulated). Once S_V was determined, the specific intensity normal to the surface was determined using the conversion factor

$$I_{0V} = \frac{2.346 \times 10^8 \text{ ergs}^{-1} \text{ cm}^{-2} \text{ Å}^{-1} \text{ sr}^{-1}}{1 - (x/3)}$$

for a 1 $R_\odot$ star with $V = 0$. This factor is based on (1) a flux 3.75×10^{-9} ergs cm^{-2} s^{-1} Å^{-1} in the V band for a $V = 0$ star, (2) the solar radius (6.96×10^{10} cm), and (3) the conversion from total monochromatic energy in the outgoing direction to specific intensity, which introduces factors of π and $1 - (x/3)$ from integration over solid angle.

After the perpendicular surface brightness of each surface element had been determined, an orbital inclination i was chosen and the light and color curves were computed by integrating over all elements visible to the observer at each observed phase. The result was the specific intensity times the projected area, which was converted to a physical flux at a fiducial distance by dividing by the square of that distance. The assumed distance to the system was then adjusted to give the best match between the theoretical and observed light curves. After some experimentation with interactive fitting, we constructed a program that automatically converges the light-curve fits by adjusting three parameters, namely, i, $T_{eff,0}$, and the luminosity of the primary L_1. The convergence was controlled by an inefficient but robust "brute force" technique that thoroughly surveyed the surrounding parameter space at each iteration. The masses were chosen at the start of each calculation and left fixed during the optimization.

Before fitting the data, we corrected them for a reddening $E(B - V) = 0.045$ mag, estimated by Schlegel et al. (1998). The $V - I$ colors were corrected using $E(V - I)/E(B - V) = 1.35$, a value taken from He et al. (1995). Including these corrections raised $T_{eff,0}$ by ~ 150 K.

To check the program, we used results from Bochkarev et al. (1979), who computed light-curve amplitudes for Roche lobe–filling secondaries. We adjusted the limb- and gravity-darkening parameters in our program to match their choices, turned off the external illumination, and used a simplified version of the surface brightness procedures to match their parameterization. With these modifications, our code reproduced their tabulated light-curve amplitudes to within a few thousandths of a magnitude.

For each model, the secondary's velocity amplitude K_2 followed from the fixed masses, the optimized inclination, and the known orbital period. However, the amplitude could be affected by nonuniform contributions to the line spectrum across the secondary. To establish a crude upper limit to this effect, we also computed a quantity K_2(back), a radial velocity amplitude that included only contributions from surface elements that were not externally illuminated. The weight of each element in the velocity average was proportional to its contribution to the light.

5. RESULTS OF THE MODELING

We computed optimized light curves for primary masses M_1 of 1, 1.4, 2, and 2.8 $M_\odot$ and secondary masses M_1 of 0.1, 0.2, 0.3, 0.5, 0.7, 0.9, and 1.2 $M_\odot$, constraining M_2 to be less than M_1. (Exploratory models with smaller M_1 did not come close to matching the observed K_2, so we did not explore smaller values of M_1 systematically.) All these combinations gave similarly good fits to the light and color curves, the curves in Figure 4 being typical. From the good fits, we conclude (1) that the model appears basically valid and (2) that the photometry alone carries essentially no information on the masses. Table 5 gives a sampling of model fits; they are chosen to give either a predicted K_2 or K_2(back) within 3 σ of the observed value.

Other features of the results are:

1. The secondary's $T_{eff,0}$ is constrained to a very narrow range, the extremes in all the models being 5570 and 5740 K. This is consistent with the spectral type.

2. The inferred distance is almost entirely determined by the secondary's assumed mass, because for a fixed P_{orb} in the Roche geometry, the secondary star's radius $R_2 \sim M_2^{1/3}$ and the surface brightness is fixed by the color. The distance can be expressed as $(2.2 \text{ kpc})(M_2/M_\odot)^{1/3}$.

3. L_1 varies over a rather limited range from 1.5 to 4 $L_\odot$. It is affected most strongly by M_1, because the binary separation increases

TABLE 5
Selected Light-Curve Fit Parameters

| M_1 ($M_\odot$)	M_2 ($M_\odot$)	i (deg)	K_2 (km s^{-1})	K_2 (back) (km s^{-1})	L_1 ($L_\odot$)	$T_{\rm eff,0}$ (K)	d (pc)
$x = 0.5,\ \alpha = 0.08$
2.00......................	0.20	34.0	241	260	2.63	5648	1281
2.00......................	0.50	37.3	240	263	2.48	5679	1726
2.00......................	0.70	39.1	238	264	2.45	5692	1934
2.00......................	0.90	42.5	243	273	2.37	5707	2108
2.00......................	1.50	48.6	238	272	2.34	5728	2532
2.80......................	0.10	31.0	259	274	3.65	5609	1035
2.80......................	0.30	34.1	270	291	3.29	5650	1465
2.80......................	0.50	35.9	270	294	3.17	5668	1727
2.80......................	0.70	37.4	269	295	3.10	5680	1930
2.80......................	0.90	38.5	266	295	3.08	5687	2101
2.80......................	1.50	44.6	272	309	2.93	5715	2507
$x = 0.0,\ \alpha = 0.08$
2.00......................	0.20	34.2	243	261	2.98	5604	1268
2.00......................	0.50	36.6	236	259	2.84	5638	1712
2.00......................	0.70	37.8	231	256	2.82	5651	1921
2.00......................	1.50	48.0	236	270	2.57	5708	2524
2.80......................	0.10	32.8	273	289	3.92	5577	1022
2.80......................	0.30	34.5	272	294	3.70	5607	1450
2.80......................	0.50	35.7	269	292	3.60	5626	1712
2.80......................	0.70	36.7	265	290	3.56	5638	1915
2.80......................	0.90	37.7	262	289	3.52	5649	2087
2.80......................	1.50	45.8	277	315	3.17	5698	2493
$x = 0.5,\ \alpha = 0.00$
1.00......................	0.70	61.1	224	259	1.19	5733	1929
1.40......................	0.20	39.5	238	259	1.72	5684	1267
1.40......................	0.30	43.6	248	271	1.61	5702	1442
1.40......................	0.50	48.3	249	278	1.56	5716	1709
2.00......................	0.10	36.0	262	279	2.38	5655	1023
2.00......................	0.20	38.1	267	288	2.24	5674	1273
2.00......................	0.30	39.7	268	291	2.17	5685	1449
2.00......................	0.50	44.7	279	307	2.03	5706	1709
2.00......................	0.70	48.0	280	312	1.98	5715	1912
2.00......................	0.90	50.9	279	315	1.96	5722	2084
2.00......................	1.20	55.9	279	319	1.94	5728	2305
$x = 0.75,\ \alpha = 0.08$
2.00......................	0.30	34.7	239	258	2.38	5681	1467
2.00......................	0.70	39.1	238	264	2.27	5709	1942
2.00......................	1.20	44.6	236	269	2.24	5728	2344
2.00......................	1.50	47.2	233	266	2.25	5736	2542
2.80......................	0.10	30.4	255	270	3.40	5634	1043
2.80......................	0.30	33.5	266	286	3.06	5669	1474
2.80......................	0.50	35.4	268	290	2.94	5686	1737
2.80......................	0.70	37.1	268	293	2.88	5698	1940
2.80......................	0.90	38.5	266	294	2.85	5706	2111
2.80......................	1.50	43.4	266	302	2.80	5725	2518
$x = 0.50,\ \alpha = 0.16$
2.80......................	0.10	29.0	244	257	3.93	5573	1036
2.80......................	0.30	31.0	248	266	3.66	5608	1468
2.80......................	0.50	32.8	250	270	3.50	5633	1732
2.80......................	0.70	34.3	250	272	3.42	5649	1936
2.80......................	0.90	35.3	247	272	3.39	5659	2108
2.80......................	1.50	38.1	239	270	3.37	5682	2524
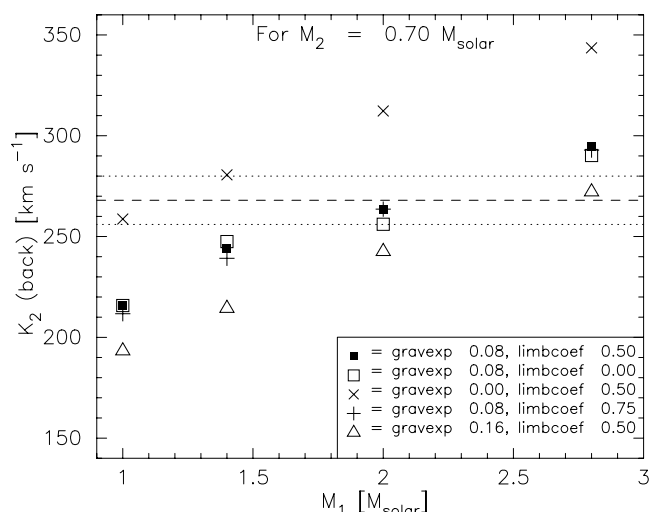
Fig. 7.—Some results from fitting models to the light curves. The velocity amplitude K_2(back), computed for the unilluminated portion of the secondary star, is plotted against the primary mass M_1 in solar masses. Computations for a secondary mass $M_2 = 0.7\ M_\odot$ are shown, but this choice makes little difference to the outcome (see text). The symbols represent choices for limb and gravity darkening; the horizontal dashed line is the observed K_2, and the dotted lines are drawn at $\pm 3\ \sigma$. Note that primary star masses below the Chandrasekhar limit are possible in the context of the models, but require low gravity darkening and the suppression of the radial velocity signal from illuminated portions of the secondary.

with M_1 at a constant P_{orb}, forcing the primary to shine more brightly to maintain a given heating effect at the secondary's face.

4. For a fixed M_2, K_2(back) exceeds K_2 by a nearly constant amount. At $M_2 = 0.7\ M_\odot$, the difference is ~ 25 km s^{-1}, while for $M_2 = 0.1\ M_\odot$ the difference drops to ~ 15 km s^{-1}.

5. K_2 is almost independent of M_2.

6. K_2 is nearly independent of the choice of limb-darkening coefficient but is strongly affected by gravity darkening, in the sense that increased gravity darkening decreases K_2. The stronger the gravity darkening, the darker the back side of the secondary becomes, which results in a more face-on inclination and hence a lower K_2.

7. The only models that come close to matching the observed $K_2 = 268 \pm 4$ km s^{-1} have large values of M_1. The models with $M_1 = 1\ M_\odot$ can only be made to fit if the gravity darkening is reduced to zero *and* the observed K_2 is identified with K_2(back). With the standard assumptions, models with M_1 at or below the Chandrasekhar limit fit the observed light curves poorly. Figure 7 illustrates this; it shows K_2(back) as a function of M_1 for a run of models with $M_2 = 0.7\ M_\odot$.

The last item is obviously provocative, but the large value of L_1 is also unexpected and suggestive. A luminosity of $\sim 2\ L_\odot$ is very high for a white dwarf and implies an effective temperature $\sim 50{,}000$ K (Bergeron et al. 1995). At this temperature there should be a strong ionizing flux, and in other close binaries harboring such hot white dwarfs this creates chromospheric emission from the illuminated face of the secondary. To estimate the magnitude of the effect in this system, we scaled the results from the 0.7 day WD + M3V binary EUVE 2013+400, in which the white dwarf is $\sim 50{,}000$ K (Thorstensen et al. 1994), and found that a similar white dwarf in this system would create emission at Hα with ~ 3 Å equivalent width (EW). Our observations show no hint of emission; the easily detected Hα absorption line has an EW of ~ 2 Å. In any case, the white dwarfs observed in magnetic CVs are typically much cooler than this, averaging only $\sim 16{,}000$ K

(Sion 1999). On both these grounds it seems unlikely that a normal white dwarf is powering the heating effect.

The implied mass is large because the heating model requires a low inclination. One natural suggestion for increasing i, and hence lowering M_1, is to add a source of steady light to the system, as would be expected from the primary. However, as noted earlier, the observed colors from the near-ultraviolet to the mid-infrared are all nicely matched by pure G-star atmospheres. We tried adding light artificially, and of course this increased the inclination, but unless the added light was also tuned to be almost exactly the color of the secondary, the added light destroyed the color match. In particular, adding any significant amount of light similar in color to a hot white dwarf completely destroyed the agreement between the observed and modeled colors.

6. DISCUSSION

What are we to make of this star? Except for the unusual discovery channel, the evidence available to Bond et al. (2002) showed a typical AM Her–type cataclysmic binary, yet since then it has shown a very different face, most likely because mass transfer has ceased, at least for the time being. There is nothing in the minimum-light spectrum to suggest that it is a cataclysmic binary; in particular, there are no emission lines. Even at deep minimum, AM Her stars such as EF Eri still show emission (see, e.g., Wheatley & Ramsay 1998).

The early spectral type of the secondary is also unusual. Beuermann et al. (1998) compiled the spectral types of CV secondaries as a function of P_{orb}, and found that for orbital periods $P_{orb} < 3$ hr, nearly all were consistent with main-sequence expectations, while for $P_{orb} > 3$ hr, secondaries were either near the main sequence or *cooler* than expected. At the 4.75 hr period of FIRST 1023+0038, the spectral type of a secondary obeying the main-sequence mass/radius/spectral type relation would be near M2, *much* cooler than observed, so FIRST 1023+0038 lies on the "wrong" side of the trend line. Recently, Thorstensen et al. (2002a, 2002b) drew attention to two shorter period systems that also show anomalously warm secondaries, namely, EI UMa ($P = 64$ minutes) and QZ Ser ($P = 2.0$ hr). The explanation advanced in those papers was that these objects arose from systems in which mass transfer began after the secondary had undergone some nuclear evolution. In QZ Ser, this is corroborated by an apparent enhancement of the Na abundance, since Na is bred out of Ne at temperatures consistent with H burning in the CNO cycle. The early spectral type and strong NaD line in FIRST 1023+0038 suggest that the secondary has undergone some nuclear evolution in this system as well. The Bond et al. (2002) spectrum does show H emission, so H-burning evidently did not complete in the material that is currently exposed on the secondary's surface.

The lack of emission lines and the excellent fit to a pure heating effect light curve at low inclination presents the most severe challenges to understanding. Here are four scenarios that might explain the observations.

Malevolent starspots.—The constraints from the light-curve model might be relaxed or removed altogether if there were extensive starspots with just the right distribution to mimic the observations. Starspots can cause strong secular variations in the light curves of rapidly rotating, late-type stars; the secondary in V471 Tau (Ibanoglu 1989) is a particularly striking example. We have not attempted to model this effect here, as the parameter space becomes dauntingly large. Starspots may play some role; the light curves shown by Woudt et al. (2004), which were

taken about a year before ours, show an asymmetry that we do not observe. As a main driver for the light curve, starspots are unattractive because they would have to be fortuitously arranged to create a false heating effect in both the light and color curves.

Residual heat.—If the heat absorbed by the secondary were retained and reemitted over a long timescale, one could get by with a much less luminous primary. We think this is unlikely, because externally irradiated stellar atmospheres are observed to respond rapidly to changes in the irradiating flux. In HZ Herculis, for example, the light curve shows complex modulations in synchrony with the 35 day disk precession period (Gerend & Boynton 1976).

A triple system.—If there were another late-type star in the system with nearly the same color as the observed secondary, it would allow the inclination to be higher and the inferred secondary mass to be lower. However, there is no evidence for a stationary line system, so we regarded this as unlikely. Such a contribution might lurk below our spectral resolution, but mixing in G-star light at the systemic velocity would increase the true K_2 still further.

A massive, invisible primary.—The data are naturally fit by an invisible massive primary that emits about 2 $L_\odot$, and the absence of emission lines from the secondary's irradiated atmosphere suggests that the intercepted radiation is thermalized deep within the secondary's atmosphere. The system does not resemble any known cataclysmic at minimum light. Thus, the prima facie evidence suggests that the primary is not a white dwarf, and hence FIRST 1023+00 is not a cataclysmic binary. If the primary is not a white dwarf, what is it?

One attractive explanation is that the primary is a neutron star, so the system is similar to a low-mass X-ray binary. The strong $\lambda 4686$ line in the Bond et al. (2002) high-state spectrum is consistent with an X-ray binary. However, the lack of any known X-ray source in the vicinity presents a vexing problem. The duty cycle for active mass transfer could be short, but at the inferred low inclination and modest distance (for an X-ray binary) it is difficult to see how any substantial X-ray source could have remained unnoticed. On the positive side, transient X-ray sources are often observed to have quiescent X-ray luminosities comparable to that inferred for the primary star (Menou et al. 1999).

A black hole primary would be even more exotic, and in this case the large velocity amplitude and low inferred inclination would be explained very naturally. Getting $\sim$2 $L_\odot$ out of the compact object without creating any emission lines could be problematic in that case.

The system does vaguely resemble V616 Mon (Gelino et al. 2001), but in that case the secondary does not show a clear heating effect. It is interesting that the primary in V616 Mon is evidently a black hole that "turns off" almost entirely in quiescence, while neutron star transients generally continue to emit at a low level after they fade (Menou et al. 1999).

To summarize, there does not seem to be any simple, plausible model for this object that does not present further difficulties. Continued optical monitoring and a sensitive search for X-ray emission might help resolve these issues.

REFERENCES

Bergeron, P., Wesemael, F., & Beauchamp, A. 1995, PASP, 107, 1047
Bessell, M. S., Castelli, F., & Plez, B. 1998, A&A, 333, 231
Beuermann, K., Baraffe, I., Kolb, U., & Weichhold, M. 1998, A&A, 339, 518
Bochkarev, N. G., Karitskaia, E. A., & Shakura, N. I. 1979, AZh, 56, 16
Bond, H. E., White, R. L., Becker, R. H., & O'Brien, M. S. 2002, PASP, 114, 1359
Gelino, D. M., Harrison, T. E., & Orosz, J. A. 2001, AJ, 122, 2668
Gerend, D., & Boynton, P. E. 1976, ApJ, 209, 562
He, L., Whittet, D. C. B., Kilkenny, D., & Spencer Jones, J. H. 1995, ApJS, 101, 335
Hendry, P. D., & Mochnacki, S. W. 1992, ApJ, 388, 603
Ibanoglu, C. 1989, Ap&SS, 161, 221
Jacoby, G. H., Hunter, D. A., & Christian, C. A. 1984, ApJS, 56, 257
Kurtz, M. J., & Mink, D. J. 1998, PASP, 110, 934
Landolt, A. U. 1992, AJ, 104, 340
Lucy, L. B. 1967, Z. Astrophys., 65, 89
Menou, K., Esin, A. A., Narayan, R., Garcia, M. R., Lasota, J.-P., & McClintock, J. E. 1999, ApJ, 520, 276
Pickles, A. J. 1998, PASP, 110, 863

Schlegel, D. J., Finkbeiner, D. P., & Davis, M. 1998, ApJ, 500, 525
Sion, E. M. 1999, PASP, 111, 532
Szkody, P., et al. 2003, AJ, 126, 1499
Thorstensen, J. R., Fenton, W. H., Patterson, J. O., Kemp, J., Halpern, J., & Baraffe, I. 2002a, PASP, 114, 1117
Thorstensen, J. R., Fenton, W. H., Patterson, J. O., Kemp, J., Krajci, T., & Baraffe, I. 2002b, ApJ, 567, L49
Thorstensen, J. R., Fenton, W. H., & Taylor, C. J. 2004, PASP, 116, 300
Thorstensen, J. R., Vennes, S., & Shambrook, A. 1994, AJ, 108, 1924
Tonry, J., & Davis, M. 1979, AJ, 84, 1511
Van Hamme, W. 1993, AJ, 106, 2096
Warner, B. 1995, Cataclysmic Variable Stars (Cambridge: Cambridge Univ. Press)
Wheatley, P. J., & Ramsay, G. 1998, in ASP Conf. Ser. 137, Wild Stars in the Old West: Proceedings of the 13th North American Workshop on Cataclysmic Variables and Related Objects, ed. S. Howell, E. Kuulkers, & C. Woodward (San Francisco: ASP), 446
Woudt, P. A., Warner, B., & Pretorius, M. L. 2004, MNRAS, 351, 1015

Note added in proof.—Brief spectroscopic observations obtained in 2004 November and 2005 March showed the system continuing in a low state. The radial velocities from these observations refine the absorption-line ephemeris (see Table 4) to $T_0 =$ HJD 2,453,073.9305(5) and $P = 0.1980959(5)$ days. The conclusions of the paper are not affected.